Computers & Industrial Engineering 156 (2021) 107235

Contents lists available at ScienceDirect

Computers & Industrial Engineering

journal homepage: www.elsevier.com/locate/caie

Monitoring scheme for early detection of coronavirus and other respiratory virus outbreaks

Salah Haridy [a,c,*], Ahmed Maged [b,c], Arthur W. Baker [d,e], Mohammad Shamsuzzaman [a], Hamdi Bashir [a], Min Xie [b,f]

[a] Department of Industrial Engineering and Engineering Management, College of Engineering, University of Sharjah, Sharjah, United Arab Emirates
[b] Department of Systems Engineering and Engineering Management, City University of Hong Kong, Kowloon, Hong Kong SAR, China
[c] Benha Faculty of Engineering, Benha University, Benha, Egypt
[d] Division of Infectious Diseases, Duke University School of Medicine, Durham, NC, USA
[e] Duke Center for Antimicrobial Stewardship and Infection Prevention, Durham, NC, USA
[f] School of Data Science, City Univeristy of Hong Kong, Hong Kong SAR, China

ARTICLE INFO

Keywords:
Coronavirus
COVID-19
Monitoring
Statistical Process Control
Control Chart
Outbreak Detection

ABSTRACT

In December 2019, an outbreak of pneumonia caused by a novel coronavirus (severe acute respiratory syndrome coronavirus 2 [SARS-CoV-2]) began in Wuhan, China. SARS-CoV-2 exhibited efficient person-to-person transmission of what became labeled as COVID-19. It has spread worldwide with over 83,000,000 infected cases and more than 1,800,000 deaths to date (December 31, 2020). This research proposes a statistical monitoring scheme in which an optimized np control chart is utilized by sentinel metropolitan airports worldwide for early detection of coronavirus and other respiratory virus outbreaks. The sample size of this chart is optimized to ensure the best overall performance for detecting a wide range of shifts in the infection rate, based on the available resources, such as the inspection rate and the allowable false alarm rate. The effectiveness of the proposed optimized np chart is compared with that of the traditional np chart with a predetermined sample size under both sampling inspection and 100% inspection. For a variety of scenarios including a real case, the optimized np control chart is found to substantially outperform its traditional counterpart in terms of the average number of infections. Therefore, this control chart has potential to be an effective tool for early detection of respiratory virus outbreaks, promoting early outbreak investigation and mitigation.

1. Introduction

1.1. Background

In December 2019, an outbreak of mysterious pneumonia from an unidentified origin occurred in Wuhan, China. Chinese health authorities identified a novel coronavirus (severe acute respiratory syndrome coronavirus 2 [SARS-CoV-2]) that was responsible for the outbreak (World Health Organization, 2020b). Coronaviruses are a large family of viruses that cause illnesses ranging from the common cold to more severe diseases, such as middle east respiratory syndrome (MERS-CoV) and severe acute respiratory syndrome (SARS-CoV). SARS-CoV-2 exhibited efficient person-to-person transmission of what became labeled as coronavirus disease 2019 (COVID-19), which quickly led to a worldwide outbreak of potentially fatal viral pneumonia. COVID-19 has spread around the world with over 83,000,000 infected cases and more than 1,800,000 deaths to date (December 31, 2020), and further dissemination through air travel is likely (Goscé, Phillips, Spinola, Gupta, & Abubakar, 2020). As a result, the World Health Organization (WHO) declared COVID-19 a pandemic on March 11, 2020 (World Health Organization, 2020a). A timeline of crucial early events related to SARS-CoV-2 is shown in Fig. 1 (CNN Health, 2020; National Health Commission of China, 2020).

The attack rate (i.e., how rapidly the disease is spreading) of a virus is indicated by its reproductive number (R_0). A recent study estimated the R_0 for COVID-19 to be between 2.24 and 3.58 (Zhao et al., 2020). Per

* Corresponding author at: Department of Industrial Engineering and Engineering Management, College of Engineering, University of Sharjah, Sharjah, United Arab Emirates.
E-mail addresses: sharidy@sharjah.ac.ae (S. Haridy), amaged2-c@my.cityu.edu.hk (A. Maged), arthur.baker@duke.edu (A.W. Baker), mshamsuzzaman@sharjah.ac.ae (M. Shamsuzzaman), hbashir@sharjah.ac.ae (H. Bashir), minxie@cityu.edu.hk (M. Xie).

https://doi.org/10.1016/j.cie.2021.107235
Received 27 June 2020; Received in revised form 3 January 2021; Accepted 8 March 2021
Available online 16 March 2021

this estimate, on average, every case of COVID-19 would create two to three new cases, exhibiting 2 to 3 times greater transmissibility than seasonal influenza viruses (Zhang et al., 2017). Furthermore, the mortality rate of COVID-19 is currently estimated at around 3% (Wang, Horby, Hayden, & Gao, 2020). For comparison, the mortality rate of seasonal flu is less than 0.1% (Centers of Disease Control and Prevention, 2019), but the mortality rate is approximately 10% for SARS-CoV and 34% for MERS (Jiang, Rayner, & Luo, 2020). Early detection and response to epidemics and pandemics, including quarantine of patients with confirmed infections and observation of those who have had close contact with infected patients, can help to mitigate outbreaks, lowering the attack rate and the total number of deaths (Bauer, 2015). In this analysis, we present how early detection of important respiratory virus outbreaks could be achieved through use of an optimized np control chart at a worldwide network of sentinel airports to improve the quality of surveillance.

1.2. Statistical process control

Using effective surveillance tools is essential for the early detection of outbreaks of coronaviruses and other respiratory viruses. When used for outbreak detection, statistical process control (SPC) charts have been proven to be effective, easy to implement, and inexpensive (Wiemken et al., 2017; Woodall, 2006). SPC charts were originally developed by Walter Shewhart in the 1920s for monitoring production processes (Montgomery, 2019). Since the early 1990s, there has been a growing interest in applying these charts to healthcare (Ahamed, Campbell, Horan, & Rosen, 2018; Lawson, Hall, Esnaola, & Ko, 2012), including those related to the detection and monitoring of outbreaks (e.g., Baker et al. (2018); Shu, Su, Jiang, and Tsui (2014); Sogandi, Aminnayeri, Mohammadpour, and Amiri (2019); Xie, Tsui, Xie, and Goh (2010)). Sogandi et al. (2019) proposed a Bernoulli state-space model for monitoring multi-stage medical processes. The proposed model performed well under different shifts and was able to identify the out-of-control stage efficiently. Grigg (2019) discussed the problem of maintaining patient ordering according to the treatment timeline for different charts. They recommended that compromising on the fullness of presentation of the historical data is the best way to preserve patient ordering on any chart. Gould and Wang (2017) proposed an effective method for routine monitoring of safety information for programs that include blinded trials. A comprehensive literature review of the various applications of SPC charts in healthcare can be found in Suman and Prajapati (2018), Tennant, Mohammed, Coleman, and Martin (2007), and May, Simpson, Hart, Rowett, and Perrier (2009).

A control chart is a visual tool that can provide early identification of statistically significant changes in data. For effective process monitoring, several studies have proposed to optimize the parameters of different types of charts in various applications. For instance, Rahim and Sultan Khalaf (1997) presented an optimal design of exponentially weighted moving average (EWMA) chart parameters using genetic algorithms. The results showed that the optimal design reduces the false alarm probability (i.e., the probability that the control chart gives an out-of-control signal, while the process is actually in control) and is powerful in detecting serious shifts. Haridy, Wu, Khoo, and Yu (2012) proposed an algorithm for the optimal design of a Syn-np chart which combines the synthetic chart and the np chart. The proposed chart was more effective than the np chart by 73% and the synthetic by 31%. Shamsuzzaman, Khoo, Haridy, and Alsyouf (2016) proposed an optimization design of the combined Shewhart $\overline{X}$chart and EWMA chart. The charting parameters and the allocation of detection power between the elements of both charts were optimized based on the loss function. Muhammad, Yeong, Chong, Lim, and Khoo (2018) developed an algorithm for the optimization of coefficient of variation (CV) control chart. The results revealed that the proposed optimized CV chart outperforms five existing CV charts in literature in almost all scenarios.

For the early detection of outbreaks of coronaviruses and other respiratory viruses, this study proposes a monitoring scheme that utilizes an attribute chart — namely, the np chart — with optimized parameters. Furthermore, we introduce the average number of infections (*ANI*) as an effective measure of the overall detection speed of the control chart for monitoring the infection rate. Finally, the use of the proposed monitoring scheme is illustrated by different scenarios.

The proposed monitoring scheme, which is shown in Fig. 2, can be used as a monitoring tool at selected metropolitan airports where

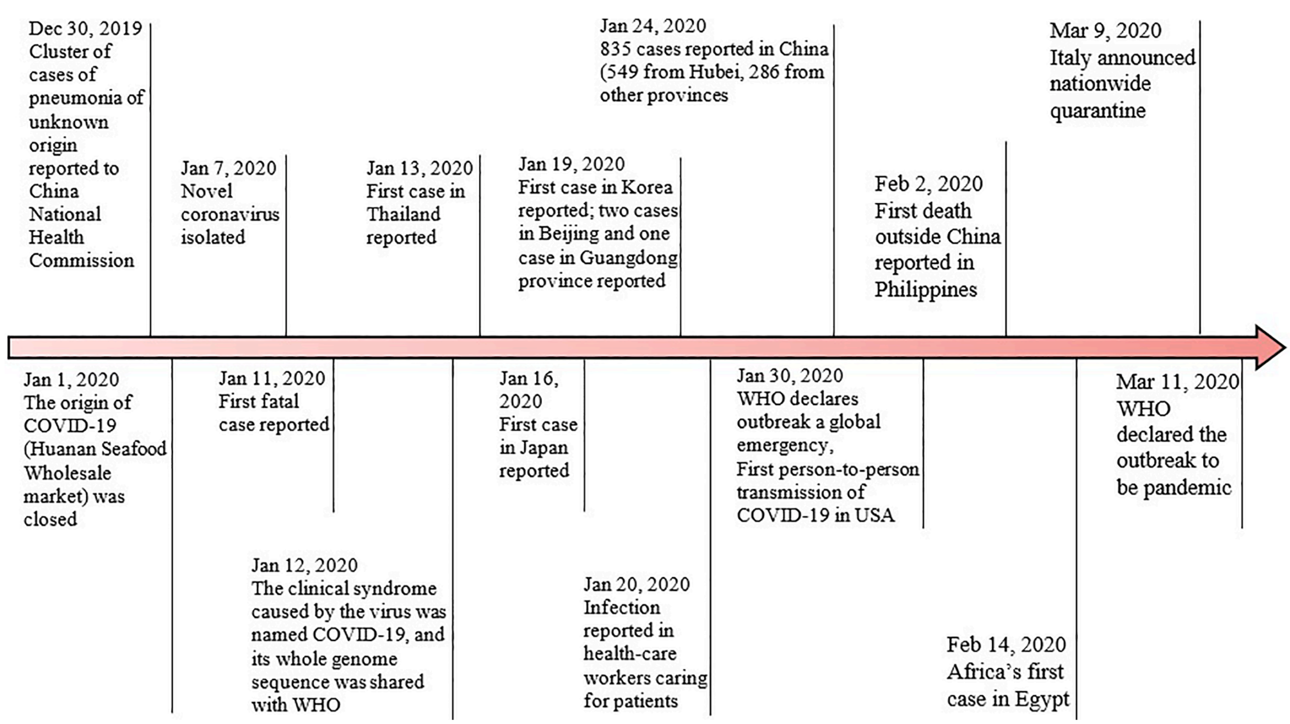

Fig. 1. A timeline of early stages of the COVID-19 outbreak.

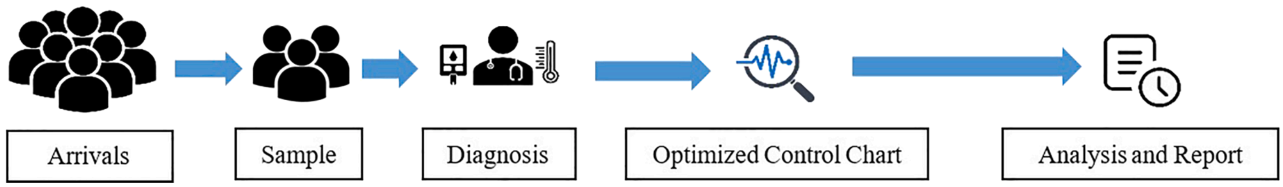

Fig. 2. The proposed monitoring scheme.

checkpoints are established. Sampling is actually a common practice in airports when 100% is impossible due to the limited resources (Bauer, 2015; Civil Aviation Authority, 2017). By the proposed scheme, airports would screen passengers to detect fevers potentially related to respiratory viruses. A typical screening procedure would include thermal screening by measuring the skin temperature using various tools, such as thermal cameras, thermal imaging, or forehead thermometer guns (Air Technology, 2020). Alternatively, if available, airports could use automated temperature screenings using artificial intelligence (GovInsider, 2020). Surveillance for other symptoms, such as cough or shortness of breath, might also be incorporated into the model to determine the likelihood of respiratory virus infection. If outbreak onset is already known to have occurred, it would be important to increase the inspection rate (i.e., increase the sample size n and decrease the sampling interval h) if 100% inspection is impossible so that a greater percentage of infected passengers could be evaluated. However, the proposed monitoring scheme can also be used continuously where either rational subgrouping or 100% inspection is adopted (Air Technology, 2020).

2. Implementation and design of the np chart

The np control chart is an attribute chart that can be used to monitor the number of infections (d) found in a sample of arriving passengers, which is assumed to follow a binomial distribution. The process being monitored is considered to be in control if d satisfies $LCL \leq d \leq UCL$, where LCL and UCL are the lower control limits and upper control limits of the np chart. In other words, if $d \leq LCL$, then a downward p shift will be signaled and if $d \geq UCL$, then an upward p shift will be signaled. However, this analysis focuses on designing a one-sided upper control chart that only detects an increase in the infection rate since decreasing the number of infections where $d \leq LCL_{np}$ is the desirable target. The np control chart process monitoring is implemented as follows:

1. A sample of n passengers is taken at the end of each sampling interval h and the number of infections, d, is counted for this sample. The policymakers could then make real-time decisions on managing the infected cases, such as quarantine.
2. The resulting d is plotted for each sample on the np chart.
3. If $d \geq UCL$, then a potential outbreak is declared and in this case, a 100% inspection is recommended. Otherwise, the process is in control, and step 1 is repeated for the next sample.

The charting parameters (i.e., n, h and UCL) need to be decided in an optimal and effective way. With the aim of carrying out the optimal design for the np chart, several specifications need to be set. The design specifications of this study are summarized below:

- p_0 is the in-control infection rate;
- τ is the allowable minimum value of the in-control average time to signal (ATS_0);
- r is the inspection rate; and
- p_{max} is the maximum out-of-control infection rate

The abovementioned specifications are commonly used to design attribute control charts (Bourke, 1991; Gan, 1993; Haridy, Rahim, Selim, Wu, & Benneyan, 2017; Reynolds & Stoumbos, 1998; Wu, Shamsuzzaman, & Pan, 2004). The in-control infection rate p_0 is assumed to be known, as it is considered to be the baseline or expected infection rate that does not require investigation. In addition, the value of τ is set based on the requirements of the false alarm rate that is deemed to be acceptable and can be managed by airports. The sampling rate r is determined according to the availability of resources such as manpower and inspection tools (e.g., thermometers and testing kits). The maximum out-of-control infection rate, p_{max}, is decided based on the shift size the authority is interested to detect.

3. The measure of performance

The performance of a control chart is often evaluated using different measures of performance. A measure called the average time to signal (ATS), which is the expected time from when a shift with a particular size occurred until the control chart indicates an out-of-control signal (i.e., outbreak), is usually recommended (Li, Zou, Gong, & Wang, 2014). Nevertheless, it is not easy to predict the size of an outbreak. Therefore, in this study, we introduce a performance measure that is the average number of infections (ANI) to evaluate the overall performance of the proposed np chart over a wide range of shifts in the infection rate. The ANI is actually a weighted average of the out-of-control ATS values over different shifts in an infection rate, hence it is a better measure for the overall performance of a control chart.

When an increasing shift in the infection rate occurs, the infection rate will change from p_0 to p. The ANI is the average number of infections that occurred over a shift range of $p_0 < p \leq p_{max}$ prior to control chart detection. The infection rate is considered to be in control when $p = p_0$ and out of control when $p_0 < p \leq p_{max}$ with a maximum infection rate at $p = p_{max}$.

If N is the number of arrivals per unit time and $ATS(p)$ is the out-of-control ATS value that corresponds to a particular infection rate p, then the ANI produced by a control chart across the p range ($p_0 < p \leq p_{max}$) can be calculated as follows:

$$ANI = N \times \int_{p0}^{p\max} p \times ATS(p) \times f_p(p)dp \tag{1}$$

where $f_p(p)$ is the probability density function of p which is assumed to follow uniform distribution in this research and can be estimated as follows:

$$f_p(p) = 1/(p_{max} - p_0) \tag{2}$$

The out-of-control $ATS(p)$ at a particular infection rate p can be calculated as follows:

$$ATS = h/[1 - \sum_{i=0}^{UCL} C_i^n (1-p)^{n-i} p^i] \tag{3}$$

N in Eq. (1) is assumed to be constant. As a result, it may be removed while not affecting the optimization design and comparative study.

4. The optimization model

This section presents the optimization model and algorithm for the np chart. The optimal design is carried out based on the four design specifications listed in Section 2. The optimization procedure to compute the optimal parameters of the np chart in minimizing *ANI* as the objective function is given as follows:

Objective : Minimize *ANI*

$$\text{Constraint}: \quad ATS_0 \geq \tau \tag{4}$$

$$\text{Constraint}: \quad r = \frac{n}{h} \tag{5}$$

Design variables : n, h and *UCL*

where n is the independent variable, while the h and *UCL* are the dependent variables on the n, r and specified value of τ, respectively. The above-mentioned model will provide the optimal values of n, h and *UCL* that will minimize *ANI* over a shift range of ($p_o \leq p \leq p_{max}$), and meanwhile, ensure that the in-control ATS_0 is greater than or equal to a predefined value of τ. The ATS_0 represents the expected time the control chart takes to give a false alarm signal. The ATS_0 of the np chart can be calculated as follows:

$$ATS_0 = h/\alpha \tag{6}$$

where α is the probability that the np chart gives an out-of-control signal when the infection rate is actually in-control. α can be determined as follows:

$$\alpha = 1 - \sum_{i=0}^{UCL} C_i^n (1-p_0)^{n-i} {p_0}^i \tag{7}$$

The optimization design of np chart is implemented as follows:

1. Specify the design specifications $p_{0,}$ $\tau_,$ r and $p_{max.}$
2. Initiate $ANI_{\min}$ variable to store the minimum value of *ANI* and set the initial value of $ANI_{\min}$ to very large number.
3. Search the optimal value of n, starting with $n = 1$ and increase its value in an increment of 1.
4. For each n, find h ($=n$ / r) that satisfies constraint (5).
   - For each pair of (n, h), find α using Eq. (6) where $ATS_0 = \tau$ (i.e., $\alpha = h / \tau$) and then the value of *UCL* using Eq. (7) so that constraint (4) can be fulfilled.
   - For the identified n, h and *UCL*, find the corresponding value of *ANI* using Eq. (1).
   - If the calculated *ANI* is less than the current ANI_{min}, replace the latter by the former and the current values of n, h and *UCL* are stored as temporary optimal solution.
5. For each trail n value, step 4 will be repeated until *ANI* cannot be further minimized. The optimization algorithm is terminated if the *ANI* keeps increasing for 60 consecutive iterations. The optimal np charting parameters n, h and *UCL* will be the values that produce the minimum *ANI*, while satisfying constraints (4) and (5).

The optimization algorithm of the np chart is summarized as shown in Fig. 3.

The above search mechanism is reliable and straightforward as the only independent design variables, n, is integral, and therefore all its possible values can be examined. It can complete the optimization design of the np chart in a few seconds of CPU time on a personal computer. In addition, the results can be used to study the effect of the sample size on the performance of the np chart. C programming language was used to code the design algorithm of the np chart. It can be obtained from authors upon request.

5. Comparative studies

This section shows the results of optimizing the charting parameters of the np chart, including n, h and *UCL*. It also conducts a comparative study between the optimized np chart and the traditional np chart for one real case and five simulated scenarios. The optimized np chart proposed in this study is named as $\text{np}_{\text{optimal}}$ chart whereas, the traditional np chart is referred to as the $\text{np}_{\text{traditional}}$ chart. Both *ANI* and *ATS* are used as measures of performance to compare the $\text{np}_{\text{optimal}}$ and $\text{np}_{\text{traditional}}$ charts and to attain a clear conclusion on how the sample size affects the performance of the monitoring chart.

5.1. Comparison under real case

This study is conducted from late December 2019 through January 2020 at an international airport with limited resources that do not allow 100% inspection. The name of the airport is not disclosed due to confidentiality reasons. The screening procedure is performed by checking the temperature using thermometer guns. A symptomatic passenger will be detected if he has a significant fever (i.e., his temperature exceeds 100.4F). Based on the available resources, the airport can only inspect 100 arrivals every hour (i.e., $r = 100$/hour) and it can handle one false alarm signal every 27 days on average (i.e., $\tau = 648$ h). The in-control infection rate that does not reflect a potential outbreak (p_o) $= 0.01$, whereas the maximum out-of-control value of the infection rate the airport is interested to detect is 10 times the in-control infection rate (i.e.,$p_{max} = 10p_o$). It is worthy to mention that the shift is assumed to follow a uniform distribution. Fixed values of n and h are used as design specification for the $\text{np}_{\text{traditional}}$ chart without any optimization. Thus, we can consider that $\text{np}_{\text{traditional}}$ inspects a sample of 100 arrivals per hour. Contradictory, both n and h are optimized under the given inspection rate r in this study. As highlighted previously, the optimal

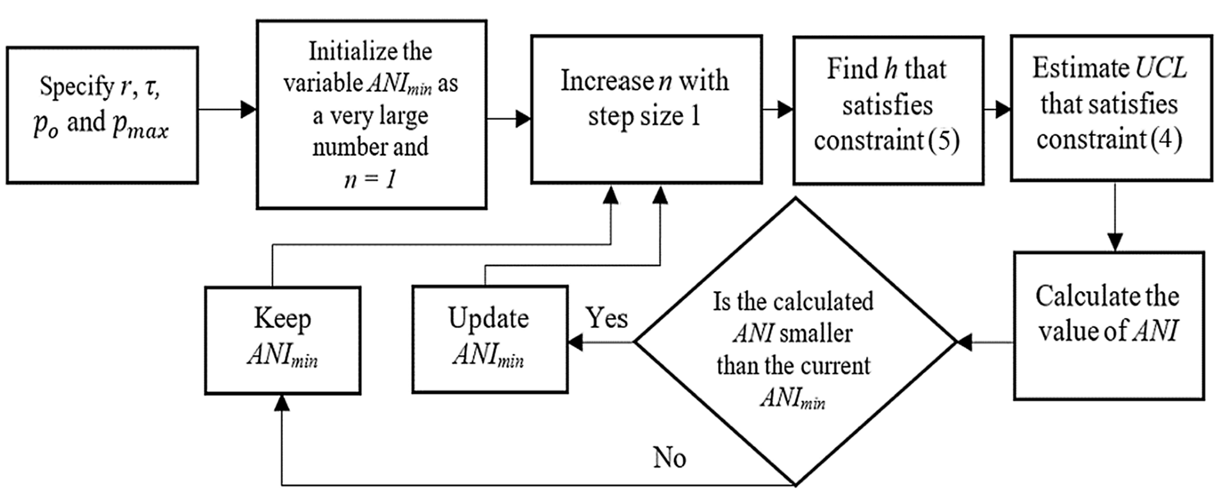

Fig. 3. The optimization algorithm of the np chart.

design of the np chart came up with the optimal combination of n, h and UCL, which produces the minimum ANI while satisfying the constraints (4) and (5). Applying the optimization algorithm, we found that the optimal charting parameters of the $np_{optimal}$ chart are to inspect a sample of size 185 (i.e., $n = 185$) at every time interval of 1.85 h (i.e., $h = 1.85$hr) using $UCL = 6$. The values of the charting parameters and the corresponding ANI values for both charts are shown below:

$np_{traditional}$ chart: $n = 100$, $h = 1$, $UCL = 5$ and $ANI = 0.2469$.
$np_{optimal}$ chart: $n = 185$, $h = 1.85$, $UCL = 6$ and $ANI = 0.1248$.

Fig. 4 shows the effect of n on the ANI values. It can be seen that the ANI values have a decay and rise pattern till they reach one point (i.e., the optimal sample size $n = 185$) where the ANI value does not go lower any further. Fig. 4 also shows that the proposed $np_{optimal}$ chart outperforms $np_{traditional}$ chart in terms of ANI under the same design specifications.

The values of ANI are compared based on a defined relative performance index (RPI) which can be calculated as:

$$RPI = \frac{ANI_{traditional} - ANI_{optimal}}{ANI_{optimal}} \quad (8)$$

RPI shows the percentage of improvement achieved by the $np_{optimal}$ chart compared to $np_{traditional}$ chart. Under the studied case, the RPI shows an improvement of 98% ($\frac{0.2469-0.1248}{0.1248} \approx 98\%$)in the ANI of the $np_{optimal}$ chart compared to that of the $np_{traditional}$ chart. One interpretation of this result is that inspecting a sample of 185 every 111 minutes can detect an outbreak almost two times faster than inspecting a sample of 100 every hour while satisfying the same constraints on the false alarm rate and inspection rate.

As shown in Fig. 4, there are several valley points (VP_i). These valley points are always the local minima on the curve of ANI against n, and ANI is actually a concave-upward function of n at these valley points. This is due to the fact that the UCL at a valley point is always the tightest, and the corresponding ATS_0 is just slightly larger than the specified τ. It also results in the smallest ANI in the neighborhood of a valley point. If the sample size n is increased by one from the sample size at a valley point, the UCL has to be increased by one in order to meet the constraint (4). Consequently, the in-control ATS_0, as well as the ANI, will increase sharply. Therefore, the optimal sample size ($n_{optimal}$) is identified as one of the valley points. For instance, the optimal sample size ($n_{optimal} = 185$) is associated with the 4th valley point (VP_4).

Moreover, the $np_{traditional}$ and $np_{optimal}$ charts are compared in terms of the out-of-control average time to signal ATS. Fig. 5 shows the performance of both np charts in terms of the normalized ATS (ATS $np_{traditional}$ / ATS $np_{optimal}$). As can be seen from Fig. 5, the $np_{optimal}$ chart is more effective than $np_{traditional}$ chart for detecting p shifts over almost the whole given range. Also, it can be noted that as the shift increases, the $np_{traditional}$ chart performs roughly similar to the $np_{optimal}$ chart. In other words, the superiority of the $np_{optimal}$ chart over the $np_{traditional}$ chart decreases with increasing the shift size in the infection rate.

5.2. Sensitivity analysis

In most processes, the process shift usually follows a specific probability distribution. However, as Siddall (1983) pointed out, if there is uncertainty about a random variable except for its bounds, then uniform distribution might be an excellent option to represent that variable. Many researchers designed control charts assuming that the process shift follows uniform distribution (Castagliola, Celano, & Psarakis, 2011; Sparks, 2000; Domangue and Patch, 1991), while others used beta distribution (Ou, Wu, & Goh, 2011) and Rayleigh distribution (Haridy, Maged, Kaytbay, & Araby, 2017; Wu, Shamsuzzaman, & Pan, 2004) to describe the process shift.

In this section, a sensitivity analysis is conducted for the case in Section 5.1 (i.e., $\tau = 648$ h, $p_0 = 0.01$, $r = 100$/hour and $p_{max} = 10p_0$) to study how the charts will perform if the estimated distribution of the p shift is not uniform. The $np_{traditional}$ and $np_{optimal}$ charts are designed for three other cases in which p shift follows a beta distribution as shown in cases 1, 2 and 3 of Table 1. The probability density function of the beta distribution can be determined as follows:

$$f_p(p) = \frac{\Gamma(a+b)}{\Gamma(a)\Gamma(b)} \cdot \frac{(p-p_0)^{a-1} \cdot (p_{max}-p)^{b-1}}{(p_{max}-p_0)^{a+b-1}} \quad (9)$$

The skewness of a beta distribution depends primarily on the parameters a and b. If ($a < b$), the probability distribution of the p shift will be skewed to right (Fig. 6(a)) and most of the shifts cluster to the lower end. If ($a > b$), the probability distribution of the p shift will be skewed to the left (Fig. 6(c)), and most of the shifts cluster to the upper end. Finally, if ($a = b$), the distribution of the p shift will be symmetric (Fig. 6 (b)). Cases 1, 2, and 3 in Table 1 serve as representatives of different types of non-uniform probability distributions of p shift.

The RPI values in Table 1 show that, under any probability distributions of p shift, the $np_{optimal}$ chart always outperforms the $np_{traditional}$ chart. The superiority of the $np_{optimal}$ chart over the np chart is more significant when $f_p(p)$ is skewed to the right (case 1). This finding is justifiable as the $np_{optimal}$ chart uses a relatively large sample size ($n = 100$), making it less sensitive for detecting large p shifts. When the beta distribution is symmetrical (case 2), it can also be observed that the RPI

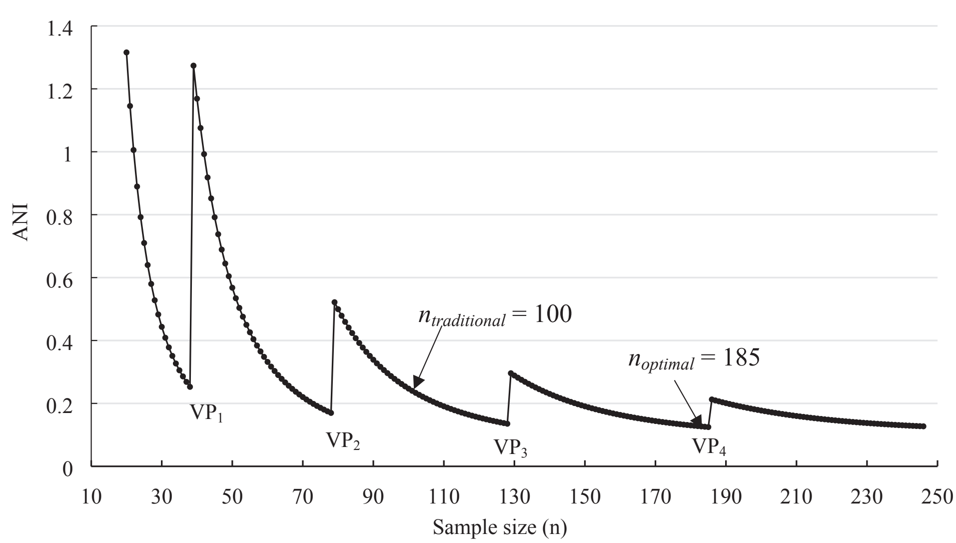

Fig. 4. The values of ANI against n.

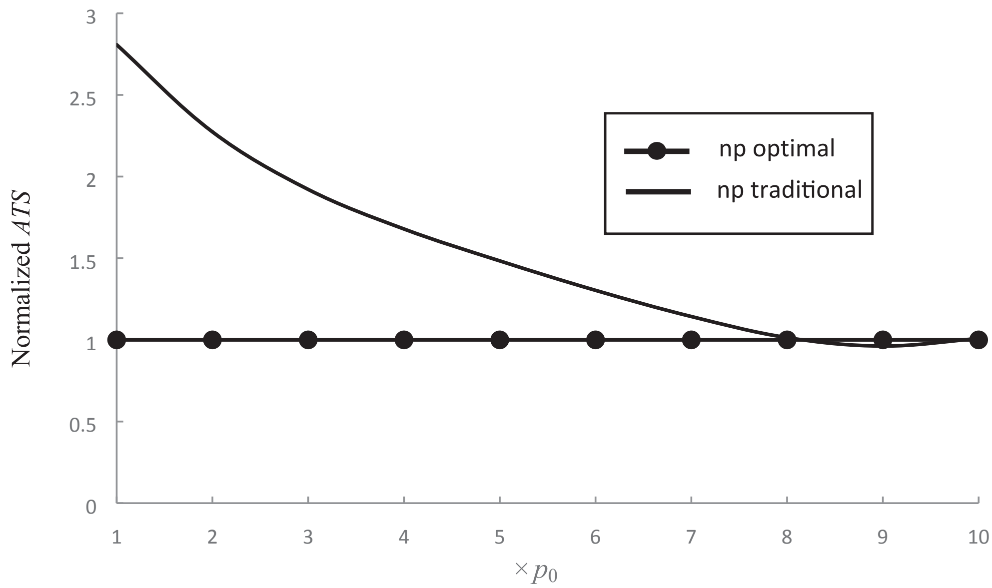

Fig. 5. The normalized *ATS* of the $np_{traditional}$ and $np_{optimal}$ charts.

Table 1
Control Charts under Different Distributions of *p* Shift.

Case	Distribution	Distribution parameters		Chart	*n*	*h*	*UCL*	*ANI*	*RPI*
		a	*b*						
1	Beta skewed to right	2	4	$np_{traditional}$ $np_{optimal}$	100 128	1 1.28	5 5	0.572 0.260	120%
2	Beta symmetrical	3	3	$np_{traditional}$ $np_{optimal}$	100 185	1 1.85	5 6	0.167 0.093	80%
3	Beta skewed to left	4	2	$np_{traditional}$ $np_{optimal}$	100 128	1 1.28	5 5	0.082 0.066	24%

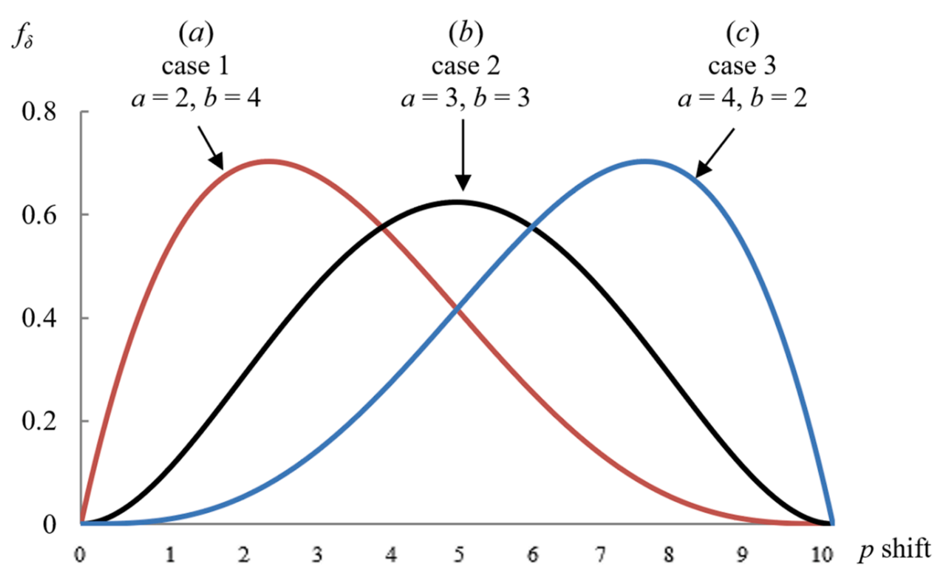

Fig. 6. Three Beta Probability Density Functions of *p* Shift.

value for case 2 when the beta distribution is symmetric is close to that of the uniform distribution in Section 5.1. It can be concluded that the $np_{optimal}$ chart always considerably outperforms the $np_{traditional}$ chart regardless of the probability distribution of the *p* shift. The distribution of *p* shift may only influence the degree of the superiority of the $p_{optimal}$ chart over the $np_{traditional}$ chart.

5.3. Comparison under different scenarios

The performance of the $np_{traditional}$ and $np_{optimal}$ charts is further compared under five more scenarios with different design specifications to demonstrate the improvement that can be achieved by optimizing n. The overall improvement is represented in terms of *RPI*, which is calculated using Eq. (8). The results are shown in Table 2.

As it can be observed from Table 2, the *RPI* values shows the superiority of the $np_{optimal}$ chart over the $np_{traditional}$ chart throughout the five scenarios. For instance, in case 4 where $r = 20$, $\tau = 900$, $p_0 = 0.03$ and $p_{max} = 5p_0$, the $np_{optimal}$ chart is able to make a reduction by 505% in the average number of infections (*ANI)* compared to the $np_{traditional}$ chart. This indicates that the $np_{optimal}$ chart is substantially more powerful for detecting the entire range of the shifts under such design specifications.

5.4. Comparison of detection speed

This section shows a comparison of the detection speed of the $np_{traditional}$ and $np_{optimal}$ charts under the same scenarios shown in Table 2. For each scenario, 30 samples with a random number of infections (d) are generated by simulation using inverse transform method. It only requires the sample size and infection rate in order to simulate d. The first 15 samples are generated to satisfy the in-control condition, and the rest are generated to be out of control. Both samples follow a binomial distribution with the same n but different infection rates (i.e., p_0 for the in-control and $i \times p_0$ for the out-of-control where i represents the increase in the shift). The values of i are indicated in Table 3. For each chart, the same sample size in Table 2 is used. For example, the first 15 samples in scenario I when using the $np_{traditional}$ chart are generated using a binomial distribution B(40, 0.03), while the other 15 samples are generated with B(40, 0.06) (i.e., using a sample size of $n = 40$ and an infection rate of $p = 2 \times 0.03 = 0.06$).

Table 3 shows the sample at which both charts will detect the shift (i.e., the detection sample). The detection sample in Table 3 indicates that the $np_{optimal}$ chart always gives an out-of-control signal faster than the $np_{traditional}$ chart. This demonstrates that the former has a better detection speed than the latter and consequently it is adopted for the early detection of an outbreak. Fig. 7 illustrates the detection speed of both the $np_{traditional}$ and $np_{optimal}$ charts under the settings given in scenarios I-V in Table 3. It is obvious that the $np_{optimal}$ chart always gives an out-of-control signal before the $np_{traditional}$ chart. This demonstrates that the former has a better detection speed than the latter and consequently it is adopted for the early detection of an outbreak.

5.5. Comparison under 100% inspection

In this section, the performance of the $np_{traditional}$ and $np_{optimal}$ charts is compared under 100% inspection using the same design specification in Section 5.1 (i.e., $\tau = 648$ h, $p_0 = 0.01$ and $p_{max} = 10p_0$) and assuming that the airport has sufficient resources to carry out such inspection. A predetermined n of 100 arrivals is used for the $np_{traditional}$ chart, while it is optimized in the design of the $np_{optimal}$ chart. In 100% inspection, optimizing the sample size n means adjusting the grouping of the inspected units (Montgomery, 2019; Reynolds & Stoumbos, 1999). The optimization model of the np chart under 100% inspection can be formulated as follows:

Objective: Minimize *ANI*
Constraint: $ATS_0 \geq \tau$
Design variables: n and *UCL*

For 100% inspection, n and *UCL* are the only parameters to be optimized as there is no sampling interval h. In addition, there is no constraint on the inspection rate r as the sampling inspection is no longer implemented.

The values of the charting parameters and corresponding *ANI* values for both $np_{traditional}$ and $np_{optimal}$ charts are indicated below:

$np_{traditional}$ chart: $n = 100$, $UCL = 2$ and $ANI = 6.4344$.
$np_{optimal}$ chart: $n = 40$, $UCL = 1$ and $ANI = 3.4073$.

The $RPI = \frac{6.4344-3.4073}{3.4073} \approx 89\%$ indicates that the $np_{optimal}$ chart has a better overall performance than the $np_{traditional}$ chart by 89%. Fig. 8 shows the performance of both np charts in terms of the normalized *ATS* (*ATS* $np_{traditional}$/*ATS* $np_{optimal}$). It is clear that the $np_{optimal}$ chart outperforms the $np_{traditional}$ chart for detecting the whole range of p shifts. In the meantime, Fig. 8 indicates that the superiority of the $np_{optimal}$ chart over the $np_{traditional}$ chart increases with increasing the shift size in the infection rate. This result is justifiable because the $np_{optimal}$ chart uses a sample size ($n = 40$) smaller than that of the $np_{traditional}$ chart ($n = 100$).

The performance of the $np_{traditional}$ and $np_{optimal}$ charts is further compared under the same five scenarios in Section 5.2 under 100% inspection. The same design specifications (τ, p_0 and p_{max}) for each scenario are used. The design specifications, charting parameter, *ANI* and *RPI* of both charts are all shown in Table 4 for each scenario.

The overall performance of the $np_{optimal}$ chart, in terms of *ANI*, is always better than, or at least equal to, that of the $np_{traditional}$ chart

Table 3
A comparison of the detection speed of the $np_{traditional}$ and $np_{optimal}$ charts.

Scenario	Chart	Shift (i)	p ($=i \times p_0$) after shift	Detection sample
I	$np_{traditional}$ $np_{optimal}$	2	0.06 0.06	23 18
II	$np_{traditional}$ $np_{optimal}$	5	0.15 0.15	22 19
III	$np_{traditional}$ $np_{optimal}$	8	0.04 0.04	23 17
IV	$np_{traditional}$ $np_{optimal}$	3	0.09 0.09	27 16
V	$np_{traditional}$ $np_{optimal}$	4	0.12 0.12	24 17

Table 2
A comparison of the $np_{traditional}$ and $np_{optimal}$ charts for sampling inspection under five different scenarios.

Scenario	Chart	p_{max}	τ	p_o	r	n	h	*UCL*	*ANI*	*RPI*
I	$np_{traditional}$ $np_{optimal}$	$5p_o$	300	0.03	40	40 119	1 2.975	5 8	0.739 0.294	151%
II	$np_{traditional}$ $np_{optimal}$	$15p_o$	300	0.03	40	40 32	1 0.8	5 4	0.331 0.241	37%
III	$np_{traditional}$ $np_{optimal}$	$15p_o$	900	0.005	120	120 164	1 1.367	4 4	0.186 0.097	92%
IV	$np_{traditional}$ $np_{optimal}$	$5p_o$	900	0.03	20	20 134	1 6.7	4 9	3.968 0.656	505%
V	$np_{traditional}$ $np_{optimal}$	$5p_o$	900	0.03	40	40 119	1 2.975	6 9	2.202 0.410	437%

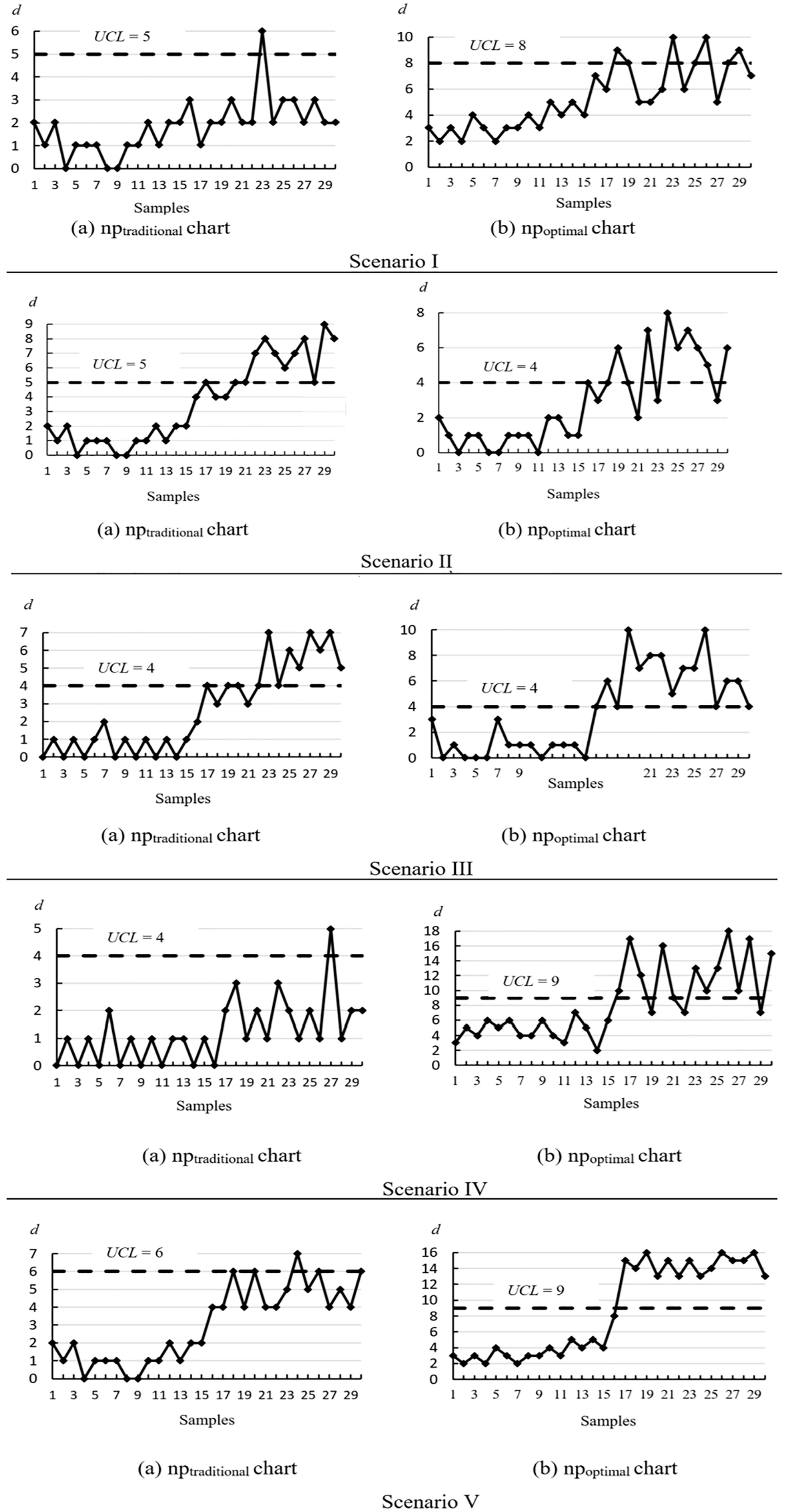

Fig. 7. A comparison of the detection speed of the two np charts under five simulated scenarios.

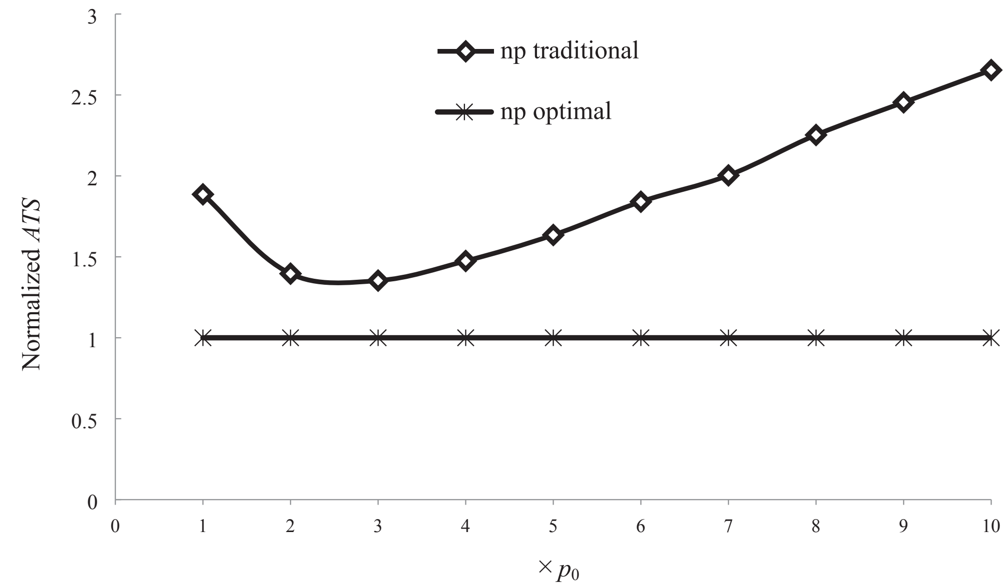

Fig. 8. The normalized *ATS* of the $np_{traditional}$ and $np_{optimal}$ charts under 100% inspection.

Table 4
A comparison of the $np_{traditional}$ and $np_{optimal}$ charts for 100% inspection under five different scenarios.

Scenario	Chart	p_{max}	τ	p_o	n	UCL	ANI	RPI
I	$np_{traditional}$ $np_{optimal}$	$5p_o$	300	0.03	40 9	2 1	5.202 4.127	26%
II	$np_{traditional}$ $np_{optimal}$	$15p_o$	300	0.03	40 9	2 1	9.020 3.310	172%
III	$np_{traditional}$ $np_{optimal}$	$15p_o$	900	0.005	120 74	1 1	4.269 3.537	20%
IV	$np_{traditional}$ $np_{optimal}$	$5p_o$	900	0.03	20 20	2 2	6.976 6.976	0%
V	$np_{traditional}$ $np_{optimal}$	$5p_o$	900	0.03	40 20	3 2	7.804 6.976	11%

across the five scenarios. *RPI* values illustrate the improvement in the overall detection effectiveness that can be achieved when the $np_{optimal}$ chart is used instead of the $np_{traditional}$ chart for each scenario.

6. Conclusion

This paper proposes a monitoring scheme for early detection of outbreaks caused by coronaviruses and other important respiratory viruses. For respiratory viruses with high transmissibility and mortality rates, such as SARS-CoV-2, early detection of important clusters of infections provides critical information to public health representatives and policymakers. In particular, early detection of respiratory virus activity at sentinel airports would allow for near real-time decisions about the potential need for specific virologic testing, patient quarantine, travel restriction, and other important outbreak investigation and mitigation measures.

The proposed monitoring scheme suggests using an optimized np control chart for monitoring the infection rate of respiratory viruses. In this scheme, clinical symptoms that are simple to monitor are used as surrogates for infection. The suggested optimized np chart is compared with the traditional np chart under both sampling inspection and 100% inspection using different settings. The results reveal that the former substantially outperforms the latter for detecting a wide range of shifts in the infection rate. Furthermore, the optimized np chart is as simple as the traditional np chart to implement. An out-of-control signal on the np chart could be a potential outbreak. The design and implementation of the developed np chart are simple, especially for healthcare practitioners without a background in control charts. Adopting the proposed monitoring scheme in sentinel airports could help identify the origin of the virus, compare infection rates at different locations, and initiate early mitigation measures.

In this research, the number of infections *d* is assumed to follow a binomial distribution. It would be worthwhile to conduct a sensitivity analysis in future research by assuming different distributions of *d*. Furthermore, the number of arrivals per unit time (*N*) is assumed to be constant; however, it might vary over time in airports. In this case, further study can be conducted employing *N* as a measure of risk by determining the exact average number of infections (*ANI*). This adjustment will allow decision-makers to manage the infected cases effectively by providing the required resources and responses, if an outbreak exists.

CRediT authorship contribution statement

Salah Haridy: Conceptualization, Methodology, Coding, Analysis, Results, Writing. **Ahmed Maged:** Methodology, Results, Writing. **Arthur W. Baker:** Methodology, Writing. **Mohammad Shamsuzzaman:** Methodology, Writing. **Hamdi Bashir:** Methodology, Writing. **Min Xie:** Writing, Editing.

Declaration of Competing Interest

The authors declare that they have no known competing financial interests or personal relationships that could have appeared to influence the work reported in this paper.

Acknowledgements

This research is supported by the University of Sharjah, UAE, under Competitive Research Project No. 18020405112. The authors sincerely thank the editor and reviewers for their constructive suggestions and valuable comments that led to a significant improvement of the paper.

Appendix A. Supplementary material

Supplementary data to this article can be found online at https://doi.org/10.1016/j.cie.2021.107235.

References

Ahamed, M. F., Campbell, D., Horan, S., & Rosen, O. (2018). Noise Reduction in the Neonatal Intensive Care Unit: A Quality Improvement Initiative. *American Journal of Medical Quality, 33*(2), 177–184. https://doi.org/10.1177/1062860617711563

Air Technology (2020). Coronavirus outbreak: safety measures at major international airports. Retrieved from https://www.airport-technology.com/features/coronavirus-measures-world-airports/.

Baker, A. W., Haridy, S., Salem, J., Ilieş, I., Ergai, A. O., Samareh, A., … Anderson, D. J. (2018). Performance of statistical process control methods for regional surgical site infection surveillance: A 10-year multicentre pilot study. *BMJ Qual Saf, 27*(8), 600–610.

Bauer, I. L. (2015). Airport Surveys at Travel Destinations—Underutilized Opportunities in Travel Medicine Research? *Journal of Travel Medicine, 22*(2), 124–129.

Bourke, P. D. (1991). *Detecting a shift in fraction nonconforming using run-length control charts with 100% inspection, 23*(3), 225–238.

Castagliola, P., Celano, G., & Psarakis, S. (2011). *Monitoring the coefficient of variation using EWMA charts, 43*(3), 249–265.

Centers of Disease Control and Prevention (2019). Past Seasons Estimated Influenza Disease Burden. Retrieved from https://www.cdc.gov/flu/about/burden/past-seasons.html.

Civil Aviation Authority (2017). Departing passenger survey. Retrieved from https://www.caa.co.uk/Data-and-analysis/UK-aviation-market/Consumer-research/Departing-passenger-survey/Departing-passenger-survey/.

CNN Health (2020). Coronavirus Outbreak Timeline Fast Facts. Retrieved from https://edition.cnn.com/2020/02/06/health/wuhan-coronavirus-timeline-fast-facts/index.htm.

Domangue, R., & Patch, S. C. J. T. (1991). Some omnibus exponentially weighted moving average statistical process monitoring schemes. 33(3), 299–313.

Gan, F. F. (1993). *An optimal design of CUSUM control charts for binomial counts, 20*(4), 445–460.

Goscé, L., Phillips, A., Spinola, P., Gupta, R. K., & Abubakar, I. (2020). Modelling SARS-COV2 Spread in London: Approaches to Lift the Lockdown. *Journal of Infection*.

Gould, A. L., & Wang, W. B. (2017). Monitoring potential adverse event rate differences using data from blinded trials: The canary in the coal mine. *Statistics in Medicine, 36*(1), 92–104. https://doi.org/10.1002/sim.7129

GovInsider (2020). How Singapore built an AI temperature tool in two weeks. Retrieved from https://govinsider.asia/innovation/covid-coronavirus-singapore-ihis-kronikare-temperature-ai/.

Grigg, O. A. (2019). The STRAND Chart: A survival time control chart. *Statistics in Medicine, 38*(9), 1651–1661. https://doi.org/10.1002/sim.8065

Haridy, S., Maged, A., Kaytbay, S., & Araby, S. (2017). *Effect of sample size on the performance of Shewhart control charts, 90*(1–4), 1177–1185.

Haridy, S., Rahim, M. A., Selim, S. Z., Wu, Z., & Benneyan, J. C. (2017). EWMA chart with curtailment for monitoring fraction nonconforming. *Quality Technology & Quantitative Management, 14*(4), 412–428.

Haridy, S., Wu, Z., Khoo, M. B., & Yu, F.-J. (2012). A combined synthetic and np scheme for detecting increases in fraction nonconforming. *Computers & Industrial Engineering, 62*(4), 979–988.

Jiang, X., Rayner, S., & Luo, M. H. (2020). Does SARS-CoV-2 has a longer incubation period than SARS and MERS? *Journal of Medical Virology*.

Lawson, E. H., Hall, B. L., Esnaola, N. F., & Ko, C. Y. (2012). Identifying worsening surgical site infection performance: Control charts versus risk-adjusted rate outlier status. *American Journal of Medical Quality, 27*(5), 391–397. https://doi.org/10.1177/1062860611428760

Li, Z., Zou, C., Gong, Z., & Wang, Z. (2014). The computation of average run length and average time to signal: An overview. *Journal of Statistical Computation and Simulation, 84*(8), 1779–1802. https://doi.org/10.1080/00949655.2013.766737

May, F., Simpson, D., Hart, L., Rowett, D., & Perrier, D. (2009). Experience with academic detailing services for quality improvement in primary care practice. *BMJ Quality & Safety, 18*(3), 225–231.

Montgomery, D. C. (2019). *Introduction to statistical quality control* (8th ed.). Wiley.

Muhammad, A. N. B., Yeong, W. C., Chong, Z. L., Lim, S. L., & Khoo, M. B. C. (2018). Monitoring the coefficient of variation using a variable sample size EWMA chart. *Computers & Industrial Engineering, 126*, 378–398. https://doi.org/10.1016/j.cie.2018.09.045

National Health Commission of China (2020). Jan 1 - Jan 30: Daily briefing on novel coronavirus cases in China. Retrieved from http://en.nhc.gov.cn/2020-02/15/c_76583.htm.

Ou, Y., Wu, Z., & Goh, T. N. (2011). A new SPRT chart for monitoring process mean and variance. *International Journal of Production Economics, 132*(2), 303–314.

Rahim, M. A., & Sultan Khalaf, S. (1997). *Optimization in quality control*. Springer.

Reynolds, & Stoumbos, Z. G. (1999). A CUSUM chart for monitoring a proportion when inspecting continuously. *Journal of Quality Technology, 31*(1), 87–108.

Reynolds, M. R., & Stoumbos, Z. G. (1998). The SPRT chart for monitoring a proportion. *IIE Transactions, 30*(6), 545–561.

Shamsuzzaman, M., Khoo, M., Haridy, S., & Alsyouf, I. (2016). An optimization design of the combined Shewhart-EWMA control chart. *The International Journal of Advanced Manufacturing Technology, 86*(5–8), 1627–1637.

Shu, L., Su, Y., Jiang, W., & Tsui, K.-L. (2014). A comparison of exponentially weighted moving average-based methods for monitoring increases in incidence rate with varying population size. *IIE Transactions, 46*(8), 798–812. https://doi.org/10.1080/0740817X.2014.894805

Siddall, J. N. (1983). *Probabilistic engineering design*. CRC Press.

Sogandi, F., Aminnayeri, M., Mohammadpour, A., & Amiri, A. (2019). Risk-adjusted Bernoulli chart in multi-stage healthcare processes based on state-space model with a latent risk variable and dynamic probability control limits. *Computers & Industrial Engineering, 130*, 699–713. https://doi.org/10.1016/j.cie.2019.02.030

Sparks, R. S. (2000). CUSUM charts for signalling varying location shifts. *Journal of Quality Technology, 32*(2), 157–171.

Suman, G., & Prajapati, D. (2018). Control chart applications in healthcare: A literature review. *International Journal of Metrology and Quality Engineering, 9*, 5.

Tennant, R., Mohammed, M. A., Coleman, J. J., & Martin, U. (2007). Monitoring patients using control charts: A systematic review. *International Journal for Quality in Health Care, 19*(4), 187–194.

Wang, C., Horby, P. W., Hayden, F. G., & Gao, G. F. (2020). A novel coronavirus outbreak of global health concern. *The Lancet, 395*(10223), 470–473. https://doi.org/10.1016/S0140-6736(20)30185-9

Wiemken, T. L., Furmanek, S. P., Carrico, R. M., Mattingly, W. A., Persaud, A. K., Guinn, B. E., … Ramirez, J. A. (2017). Process control charts in infection prevention: Make it simple to make it happen. *Am J Infect Control, 45*(3), 216–221. https://doi.org/10.1016/j.ajic.2016.09.021

Woodall, W. H. (2006). The use of control charts in health-care and public-health surveillance. *Journal of Quality Technology, 38*(2), 89–104. https://doi.org/10.1080/00224065.2006.11918593

World Health Organization. (2020a). Coronavirus disease 2019 (COVID-19) Situation Report – 25. Retrieved from https://www.who.int/docs/default-source/coronaviruse/situation-reports/20200214-sitrep-25-covid-19.pdf?sfvrsn=61dda7d_2.

World Health Organization (2020b). Coronavirus disease (COVID-19) outbreak. Retrieved from https://www.who.int/westernpacific/emergencies/covid-19.

Wu, Z., Shamsuzzaman, M., & Pan, E. S. (2004). Optimization design of control charts based on Taguchi's loss function and random process shifts. *International Journal of Production Research, 42*(2), 379–390.

Xie, Y., Tsui, K., Xie, M., & Goh, T. (2010). Monitoring time-between-events for health management. *Paper presented at the 2010 prognostics and system health management conference*.

Zhang, Q., Perra, N., Perrotta, D., Tizzoni, M., Paolotti, D., & Vespignani, A. (2017). Forecasting seasonal influenza fusing digital indicators and a mechanistic disease model. *Paper presented at the proceedings of the 26th international conference on world wide web*.

Zhao, S., Lin, Q., Ran, J., Musa, S. S., Yang, G., Wang, W., … Wang, M. H. (2020). Preliminary estimation of the basic reproduction number of novel coronavirus (2019-nCoV) in China, from 2019 to 2020: A data-driven analysis in the early phase of the outbreak. *International Journal of Infectious Diseases, 92*, 214–217. https://doi.org/10.1016/j.ijid.2020.01.050